Journal of Magnetism and Magnetic Materials 411 (2016) 91–97

Contents lists available at ScienceDirect

Journal of Magnetism and Magnetic Materials

journal homepage: www.elsevier.com/locate/jmmm

Hyperfine interaction and tuning of magnetic anisotropy of Cu doped $CoFe_2O_4$ ferrite nanoparticles

Khalid Mujasam Batoo [a,*], Dina Salah [b], Gagan Kumar [c], Arun Kumar [c], Mahavir Singh [c], M. Abd El-sadek [d], Feroz Ahmad Mir [e], Ahamad Imran [a], Daler Adil Jameel [f]

[a] King Abdullah Institute for Nanotechnology, King Saud University, P.O. Box-2455, Riyadh 11451, Saudi Arabia
[b] Department of Physics, Ain Shams University, Khalifa El-Maamon, Street, 11566 Cairo, Egypt
[c] Department of Physics, Himachal Pradesh University, Summer Hill, Shimla 171005, India
[d] Nanomaterials Lab, Physics Department, Faculty of Science, South Valley University, Qena 83523, Egypt
[e] University Science Instrumentation Centre, University of Kashmir, Srinagar 190006, India
[f] School of Physics and Astronomy, Nottingham Nanotechnology and Nanoscience Center, University of Nottingham, NG7 2RD, United Kingdom

ARTICLE INFO

Article history:
Received 18 May 2015
Received in revised form
28 February 2016
Accepted 15 March 2016
Available online 18 March 2016

Keywords:
Ferrites
Nanoparticles
Mössbauer spectroscopy
Magnetization

ABSTRACT

Ferrimagnetic oxides may contain single or multi domain particles which get converted into superparamagnetic state near a critical size. To explore the existence of these particles, we have made Mössbauer and magnetic studies of Cu^{2+} substitution effect in $CoFe_{2-x}O_4$ Ferrites (0.0, 0.1, 0.2, 0.3, 0.4, and 0.5). All the samples have a cubic spinel structure with lattice parameters increasing linearly with increase in Cu content. The hysteresis loops yield a saturation magnetization, coercive field, and remanent magnetization that vary significantly with Cu content. The magnetic hysteresis curves shows a reduction in saturation magnetization and an increase in coercitivity with Cu^{2+} ion substitution. The anisotropy constant, K_1, is found strongly dependent on the composition of Cu^{2+} ions. The variation of saturation magnetization with increasing Cu^{2+} ion content has been explained in the light of Neel's molecular field theory. Mössbauer spectra at room temperature shows two ferrimagnetically relaxed Zeeman sextets. The dependence of Mössbauer parameters such as isomer shift, quadrupole splitting, line width and hyperfine magnetic field on Cu^{2+} ion concentration have been discussed.

1. Introduction

Magnetic nanoparticles have attracted lot of attention of scientific community especially in the last two decades due to their promising and unique properties compared to their bulk counterpart [1–2]. The unique properties of these materials are because of their small size and governed by surface to volume ratio. At first, such particles reach the so-called single domain limit, predicted by Kittle in 1946 [3]. Nanostructured ferrites are having wide applications in magnetic storage devices, magnetic field sensors, drug delivery systems, microwave devices (as an isolator, tunable filter, delay line, circulator, absorber, etc.) and radio frequency devices (as high quality filters, antennas, transformer cores, etc.). At the nanoscale, ferrites display unique and interesting properties such as superparamagnetism, collective magnetic excitation, metastable cation distribution, surface spin canting effects, spin glass like behavior, etc. [4–9]. It has been found that among the various factors which affect the magnetic behavior of nanoferrite particles are their composition, crystal size, and shape [10]. Hence, in order to tune the properties of these, apart from the ferrite composition, a proper choice of the synthesis technique and specific conditions are also a key tool to achieve control of crystal growth/size and shape.

Among the various ferrite materials, Cobalt ferrite ($CoFe_2O_4$) is a promising material and has been extensively studied because of its interesting properties, such as cubic magnetocrystalline anisotropy, high coercivity, moderate saturation magnetization, high chemical stability, wear resistance, and electrical insulation [11–14]. When cobalt is involved in well-defined cobalt ferrite compound located in a surface layer, we can assume that the Co^{2+} mobility is smaller and the particle properties are less temperature dependent. The stable character of cobalt ferrite has been attributed to the extreme ion relaxation time of Co^{2+} in $CoFe_2O_4$ in comparison with the relaxation time of Co^{2+} in cobalt doped iron oxide [15]. Bulk $CoFe_2O_4$ is ferrimagnetic below the Curie temperature (T_c=860 K) [16]. At room temperature, it has saturation magnetization (M_s) of 80 emu/g and coercivity (H_c) of (1–10) kOe

* Corresponding author.
E-mail addresses: khalid.mujasam@gmail.com, kbatoo@ksu.edu.sa (K.M. Batoo).

http://dx.doi.org/10.1016/j.jmmm.2016.03.058
0304-8853/

[16–20]. It has an easy magnetization axis along [100] with magnetic saturation ($3.95\mu_B$) per formula unit at 5 K and $3.35\mu_B$ at 300 K [21]. The interactions between tetrahedral (A) and octahedral [B] sub-lattices in the spinel system (AB_2O_4) consist of inter-sublattice (A–B) super-exchange interactions and intra-sub-lattice (A–A) and (B–B) exchange interactions. Inter-sub-lattice super-exchange interactions of the cations on the (A–B) are much stronger than the (A–A) and (B–B) intra-sub-lattice exchange interactions [22]. From a molecular field model, there are six exchange parameters between tetrahedral Fe^{3+}(A), octahedral Fe^{3+}(B′) and Co^{2+}(B″) when $x=0$. It leads to antiferromagnetic exchange constants $J=-20$ K (J_{AA}, J_{AB}, $J_{AB'}$, $J_{B'B'}$, $J_{B'B''}$) except for $J_{B''B''}\approx+40$ K. When $x=0$, there are no Co^{2+} ions at the A site. In view of this, expected value of saturation magnetization is $3\mu_B$ by considering all the A-site moments parallel to one another and antiparallel to the B-site moments. This $3\mu_B$ is less than the experimentally measured value of $3.95\mu_B$. The highest measured value could be due to the contribution from orbital moments [16]. The substitution of Cu brings about a structural phase transition accompanied by the reduction in the crystal symmetry due to cooperative Jahn–Teller effect [23,24], which ultimately modifies the properties of nickel ferrite which are useful in many device applications

The aim of this work is to see (i) the effect of Cu^{2+} doping on the hyperfine fields of the two iron sites (tetrahedral: A and octahedral: B) of a cubic inverse spinel structure like Cobalt Ferrite; (ii) to study the modifications introduced in the magnetic properties of Cu^{2+} substituted grown cobalt-ferrite nanoparticles at room temperature.

2. Experiment and characterization

Nanoparticles of Cu^{2+} doped $CoFe_2O_4$ with the stoichiometric formula $CoFe_{2-x}Cu_xO_4$ (0.0, 0.1, 0.2, 0.3, 0.4, and 0.5) were prepared through auto combustion reaction method. All reagents [Ferric nitrate $Fe(NO_3)_3\cdot 9H_2O$, Cobalt nitrate $Co(NO_3)_3\cdot 6H_2O$ and anhydrous Cuprous chloride $Cu(NO_3)_2\cdot 3H_2O$, and urea $Co(NH_2)_2$ as fuel] were analytical reagent (AR) graded and were manipulated in air without protection of nitrogen or inert gas at 100 °C. According to propellant chemistry, the oxidizing and reducing valencies of different elements are as follows: C=4, H=1, O=−2, N=0, M=2, 3 etc. Generally in case of ferrites, the oxidizing valence of a divalent metal nitrate $M(NO_3)_2$ becomes −10; and that for trivalent metal nitrate $M(NO_3)_3$ becomes −15, which should be balanced by total reducing valences of fuel; urea CH_4N_2O, which adds up to +6. Hence, in order to release maximum energy, the stoichiometric composition of the redux mixture for the reaction requires $-40+6m=0$ or m=6.67 mol of urea. Thus, in order to prepare $CoFe_2O_4$, the reactants were combined in a molar proportion of 1:2:6.67 of the Co $(NO_3)_2\cdot 6H_2O$: Fe $(NO_3)_3\cdot 9H_2O$: CH_4N_2O respectively. The end product in the form of powder was annealed at 400 °C for 12 h, followed by grinding for 1 h using mortar and pestle. In order to verify the phase formation and size obtained, X-ray diffraction (XRD) studies were carried out using PANalytical X'Pert Pro X-ray diffractometer with Cu Kα ($\lambda=1.54$ Å) in the range of 20° to 80° at sweeping of 2 degrees/min, and high resolution transmission electron microscope (HRTEM-Joel 2010). The Magnetic hysteresis loops were measured at room temperature using a vibrating sample magnetometer (VSM) of Microsense, USA, with a maximum field of 40 kOe. Mössbauer spectra measurement was done in the transmission mode with 50 mCi ^{57}Co source diffused in rhodium matrix moving with constant acceleration. The spectrometer (Wissel, Germany) was calibrated by means of a standard α-Fe foil with thickness 12.5 μm and the isomer shift was expressed with respect to this standard at room temperature.

3. Results and discussion

3.1. Structural and morphological study

Fig. 1 presents the X-ray diffraction patterns along with Rietveld refined data for all the studied compositions of $CoFe_{2-x}Cu_xO_4$ (0.0, 0.1, 0.2, 0.3, 0.4, and 0.5) nanoferrites. Here, the experimental data are shown as open circles, and the calculated intensities are shown as solid line. The bottom line represents the difference between the measured and the calculated intensities. The existence of the main peaks of $CoFe_{2-x}Cu_xO_4$ are (220), (311), (222), (400), (331), (511), (400), (331), (422), (511), (440), (531), (442), (620), (533), and (622) corresponding to the angular positions at $2\theta=30.22°$, 35.61°, 37.22°, 43.35°, 47.51°, 53.72°, 57.22°, 62.77° corresponding to the cubic spinel structure with space group Fd_3m (O_h^7 *No*. 227), but we have witnessed additional peak positions at (104), (113) and (116), which correspond to an impurity phase of Fe_2O_3. The average crystallite size of the nanoparticles was determined through peak broadening technique using Scherer formula [25]:

$$t=\frac{0.9\lambda}{\beta\cos\theta} \tag{1}$$

where t is the crystallite size, β is the full width at half-maximum (FWHM) of the (311) peak, λ is the X-ray wavelength (1.54 Å) and θ is the angle of diffraction. The lattice parameter (a_{th}) of the nanoferrites was calculated by using the following relation [25]

$$a=\frac{\lambda}{2\sin\theta}\times\sqrt{h^2+k^2+l^2} \tag{2}$$

The calculated values of crystallite size (t), lattice parameter (a) and theoretical density ($\rho_{X\text{-ray}}$) for all the nanoferrites are presented in Table 1. The crystallite size was found to decrease from 40 nm to 29 nm (± 1). The lattice parameter was observed to increase with increasing Cu^{2+} substitution and is because of the large ionic radius of Cu^{2+} (0.076 nm) [26] ion compared to Fe^{3+} ions (0.067 nm) [26]. Since the Fe^{3+} ions were replaced by the copper ions therefore, the lattice expanded, and hence, the lattice constant increased. Fig. 2a shows the HRTEM micrograph for the composition, $x=0.1$, which shows that nanoparticles are agglomerated with uniform shape, and are smaller in size. The average particle size of the nanoparticles has been calculated from a TEM micrograph by calculating the perimeter a and b for each particle and then taking their average as the particles are not spherical. The particle sizes obtained have been found to match well with those estimated from XRD within an error of 1%. Fig. 2b presents the selective area electron diffraction (SAED) pattern for the composition, $x=0.1$, which shows the presence of diffused rings, which is a signature of the high crystalline order. The diffused rings have been indexed and crystallographic d value of 0.477 nm corresponding to the lattice plane (311) has been observed, which is in good agreement with the values calculated from XRD data. Fig. 2c, (for $x=0.1$) shows that the lattice fringes are parallel throughout and confirm the crystalline nature of the samples.

3.2. Magnetic properties

Fig. 3 shows the field dependent magnetization (M–H) curves for $CoFe_{2-x}Cu_xO_4$ at room temperature indicating reasonably good ferrimagnetic behavior at room temperature. The M values at 40 kOe for $x=0.0$ and 0.5 are 62.17 and 19.72 emu/g, respectively (Table 1). Since magnetization value is not saturated up to 17 kOe, saturation magnetization, M_s, was determined by extrapolating a

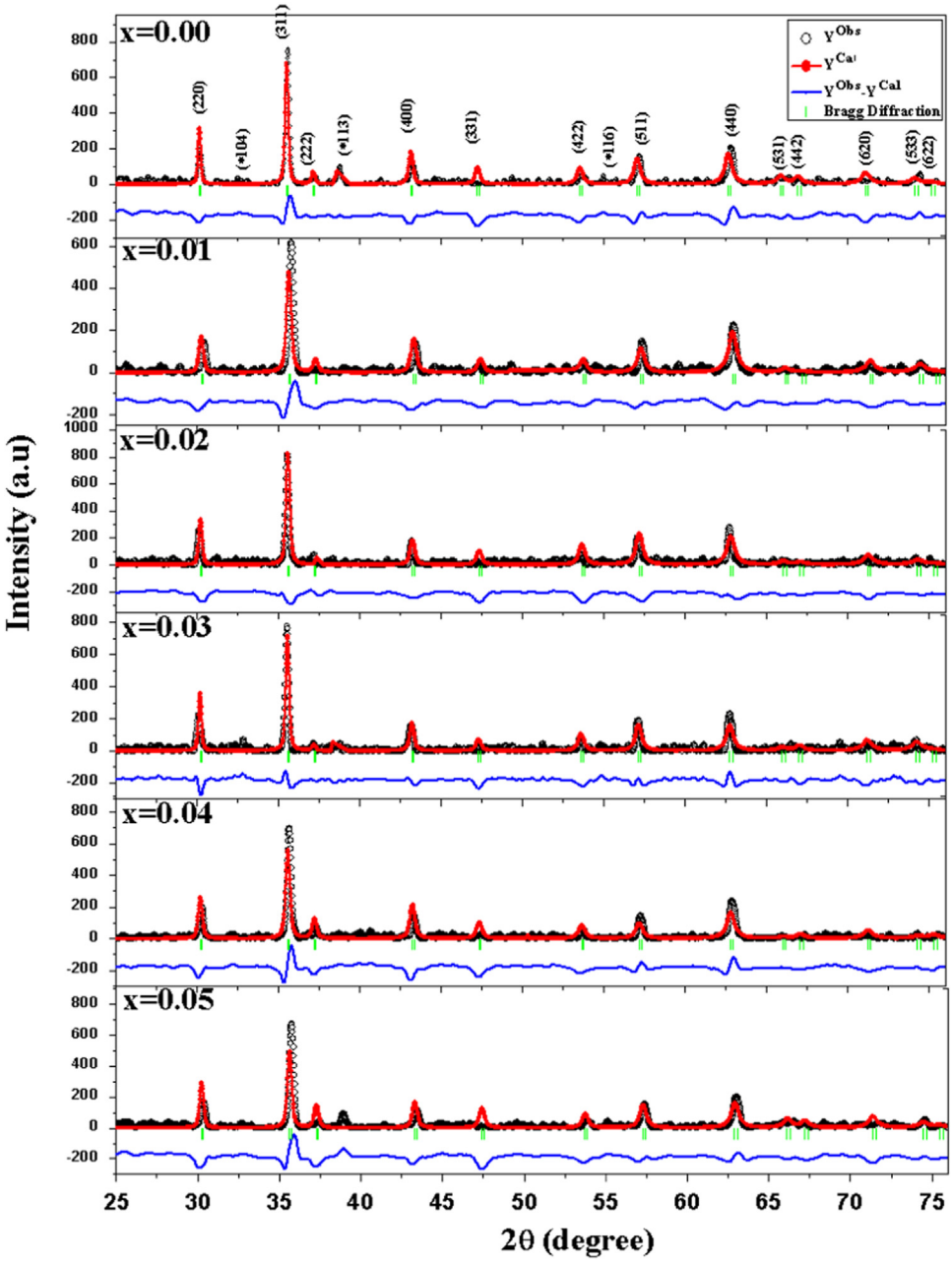

Fig. 1. XRD pattern of the $CoFe_{2-x}Cu_xO_4$ ($0.0 \le x \le 0.5$) ferrite nanoparticles.

Table 1
Presents variation of particle size (t), lattice constant (a), saturation magnetization (M_s), remenant magnetization (M_r), and coercitivity (H_c) with Cu^{2+} content.

$x \rightarrow$	0.0	0.1	0.2	0.3	0.4	0.5
t (nm)	40	38	34	32	30	29
a (Å)	8.3834	8.3835	8.3837	8.3839	8.3840	8.3843
M_s (emu/g)	62.17	39.31	41.03	32.23	30.31	19.72
M_r (emu/g)	18.38	14.9	17.3	12.6	9.01	7.63
H_c (Oe)	765.28	1131.9	1176.1	1126.4	497.3	549.06
M_r/M_s	0.30	0.38	0.42	0.39	0.30	0.39

graph of M versus 1/H to $1/H \rightarrow 0$. The thin loops illustrate the magnetic behavior of the ferrite samples. Table 1 shows the coercivity and saturation magnetization values as a function of composition. As a well-established fact, larger grains tend to consist of more magnetic domains. The magnetization caused by domain wall movement requires less energy than by domain rotation. It is easy for the domain wall movement to magnetize or demagnetize samples with larger grain size. Therefore, samples with larger grains are expected to have a low coercivity (H_c) and high saturation magnetization [18]. The relationship between coercivity and grain size can be written as:

$$H_c = a + \frac{b}{D} \tag{3}$$

where a and b are constants, and D represents the grain diameter. From Eq. (3) it is clear that the larger the size of a particle, lesser is the coercivity. As the particle size reaches a critical nano size, the particles behave as a single domain. Local magnetic anisotropy is a weak and magnetic exchange becomes important, which results in low coercivity in the magnetic nanomaterials [19]. The saturation magnetization, M_s, for the $CoFe_2O_4$ decreases with increasing percentage of Cu^{2+} ions. This behavior can be explained on the

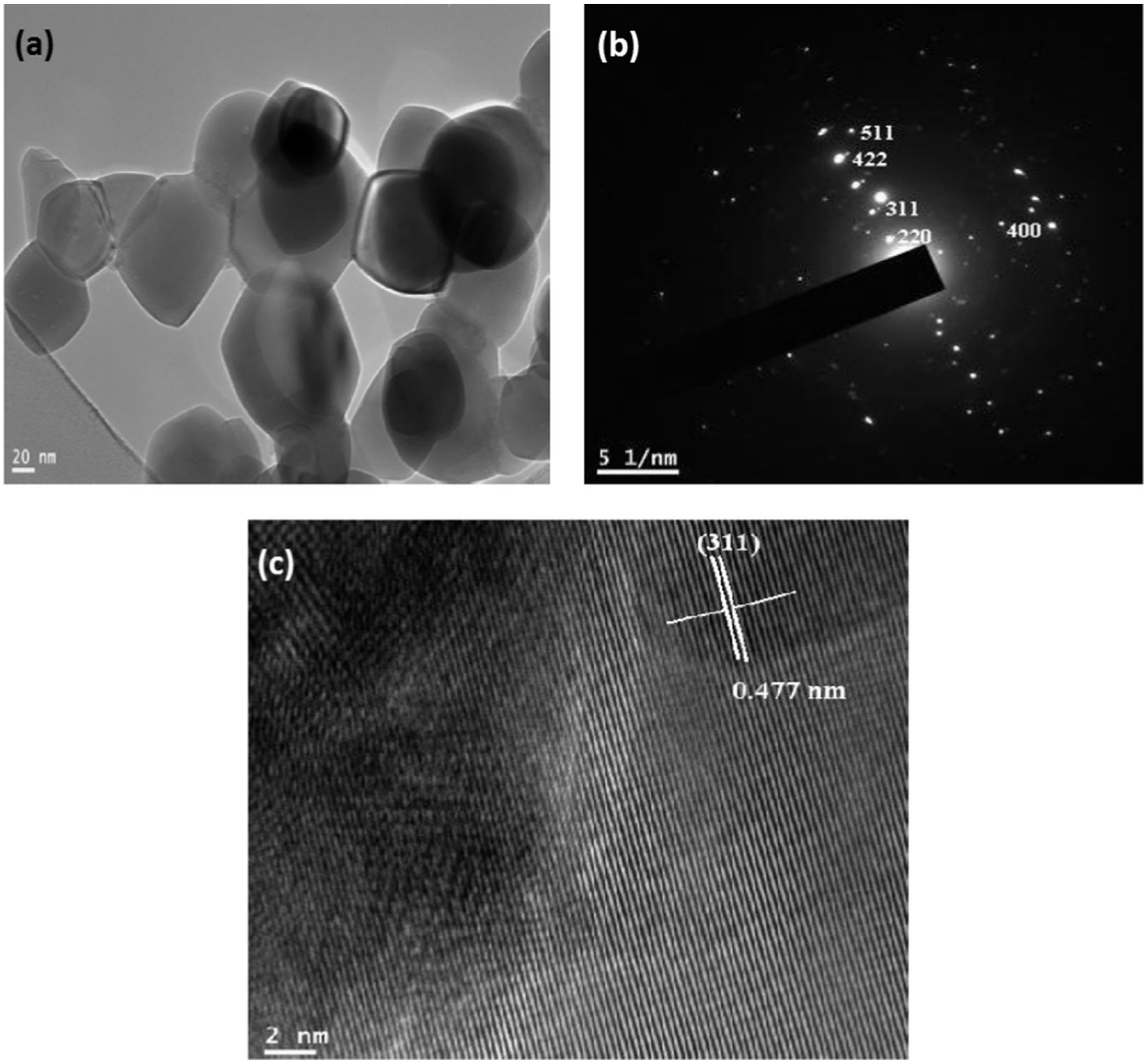

Fig. 2. (a) HRTEM micrograph for $x=0.1$, (b) selective area electron diffraction pattern (c) lattice spots.

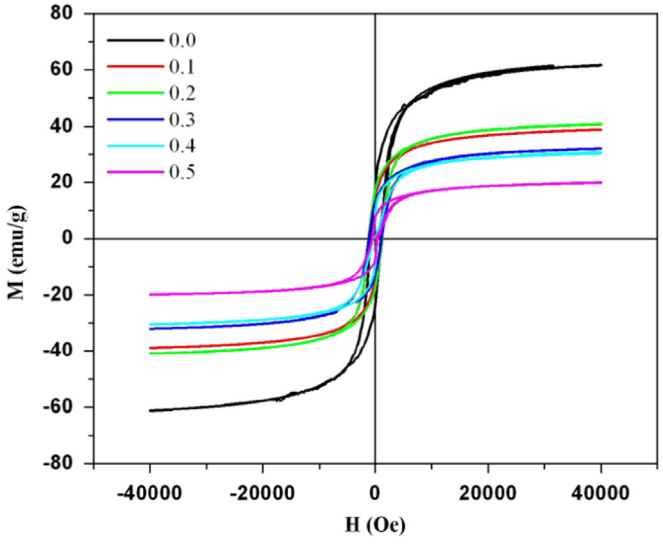

Fig. 3. Room temperature hysteresis loops for $CoFe_{2-x}Cu_xO_4$ ($0.0 \le x \le 0.5$) ferrite nanoparticles.

basis of Neel's two sublattice model. According to this model, the superexchange *A–B* interaction is the strongest interaction amongst the three interactions, *A–A*, *B–B* and *A–B*. The net magnetization is, therefore, the vector sum of the magnetization contributed by two sub-lattices A and B, i.e., $M=M_B-M_A$. When the concentration of doping is low, the Cu^{2+} ion of magnetic moment $1\mu_B$ enters the (spin-down) tetrahedral sites to replace a magnetic Fe^{2+} ion, and the magnetic moment decreases by $3\mu_B$. As the amount of Cu^{2+} ions in the tetrahedral sites reaches some saturation value, the further doping of Cu^{2+} ions begin to enter the octahedral sites rather than tetrahedral site, where they replace the Fe^{3+} ions; causing a decrease in magnetic moment by $9\mu_B$. For low doping concentration, the total magnetic moment decreases slowly, while for higher concentration, the decrease in the total magnetic moment is high [20–22].

The temperature dependence of cubic anisotropy constant for different Cu^{2+} ions substituted cobalt ferrites was determined by a "law of approach" (LA) to saturation, which describes the dependence of magnetization M on the applied magnetic field for $H \gg H_c$. The magnetization near the saturation, M_s is usually written as [23]:

$$M = M_s\left[1 - \frac{8}{105}\left(\frac{K_1}{M_s H}\right)^2\right] + kH \tag{4}$$

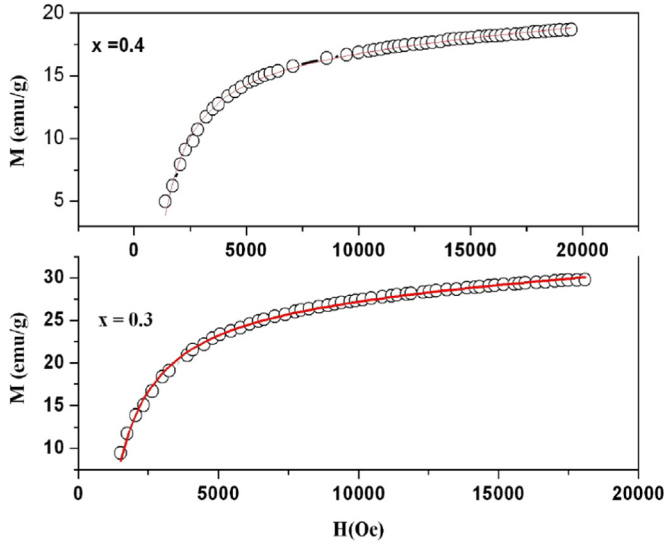

Fig. 4. Fitted *M*-*H*-curves for high magnetic field part for the composition $x=0.3$ and 0.4, respectively.

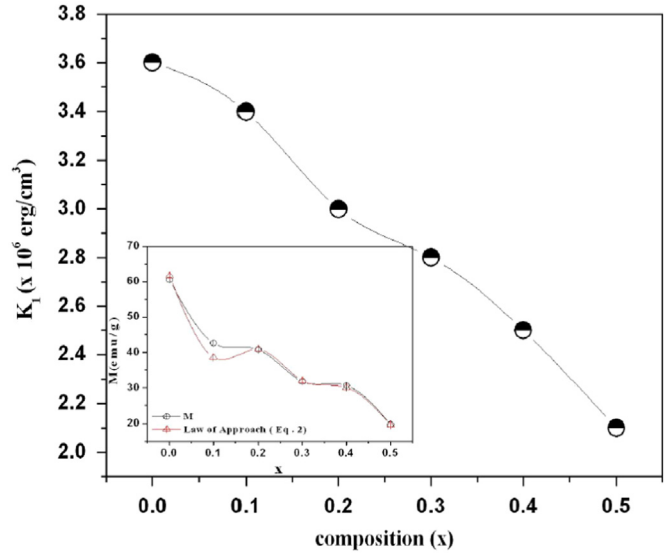

Fig. 5. Variation of anisotropy constant K_1 with magnetization with inset showing variation of magnetization and law of approach (Eq. (2)) with composition.

where the numerical coefficient 8/105 holds for random polycrystalline specimens with cubic anisotropy and K_1 is the cubic anisotropy constant. The term kH is included to take into consideration the observed increase in the spontaneous magnetization at high fields, known as the forced magnetization, with the parameter K being the high-field susceptibility. In general, the forced magnetization term is necessary to fit the hysteresis curves at higher temperatures and higher fields (shown in Fig.4). The temperature dependence of K_1, and M_s is obtained by fitting Eq. (2). As shown in inset of Fig.5 to the values of M corresponding to the high magnetic field part of the curve, e.g., using values of H above which the hysteresis loop is completely closed high field part ($10 \le h \le 30$ kOe) for Cu^{2+} substituted $CoFe_{2-x}O_4$ ($x=0.0$, 0.1, 0.2, 0.3, 0.4, and 0.5). The anisotropy constant, K_1, is found strongly dependent on composition of Cu^{2+} ions. The anisotropy constant, $K_1 \sim 3.54 \times 10^6$ erg/cm^3 for $x=0.0$, decreases to 2.3×10^6 erg/cm^3 for $x=0.5$, and can be interpreted in terms of interparticle interactions introduced by the thermal fluctuations, cation (Co^{2+}) distribution over A and B-sites of the spinel structure of Cobalt ferrite an cation vacancy or other imperfections that exert fields on Co^{2+} ions.

3.3. Mössbauer spectroscopy

Mössbauer spectra of the as-prepared $CoFe_{2-x}Cu_xO_4$ nanoparticles as a function of composition were recorded at room temperature and are presented in Fig. 6. The spectra are closely related and show a well-defined Zeeman pattern consisting of two separate sextets; one attributed to Fe^{3+} ions present at tetrahedral (A) sites having smaller isomer shift and hyperfine field, and another to the Fe^{3+} ions present at octahedral (B) sites having larger isomer shift and hyperfine field, confirming the ferrimagnetic ordering in the compounds. Based on the obtained values of isomer shifts (IS) the spectral components (shown in Table 2), it can be stated that very less ferrous (Fe^{2+}) ions are presented in the material [23]. The results indicate that the s-electron density at the Fe^{3+} nucleus is not affected too much by the Cu^{2+} substitution, since the isomer shift, for a particular nuclear transition of the Mössbauer source, is dependent only on s-electron charge density of the absorber. The results $\Delta_{IS}(A) < \Delta_{IS}(B)$ is well in agreement with the results of the other workers [25–30]. The behavior is attributed to the large bond separation of Fe^{3+}–O^{2-} for the octahedral ions compared to that of tetrahedral ions. Due to smaller overlapping of orbital's of $Fe^{3+}$and O^{2-} ions, the covalency effect is small; hence the isomer shift is large at octahedral sites.

In the present study, all the samples exhibit hyperfine Zeeman pattern, without any quadrupole splitting within the experimental error for A and B sites. The center of the Zeeman pattern does not show any significant change. The behavior can be explained on the basis that a zero quadrupole splitting is due to the presence of chemical disorder. The chemical disorder produces a distribution of electric field gradient (EFG) of varying magnitude, direction, sign, and symmetry. The resulting distribution of the quadrupole shift is represented by the equation [31]:

$$\left|\Delta E_Q\right| = 1/2\left|\Delta E_{Q0}\right|(3\cos^2\theta - 1), \tag{5}$$

Where $\left|\Delta E_Q\right|$ is the magnitude of the shift when the magnetic interaction tends to be zero and θ is the angle between axially symmetric EFG and magnetic field direction. This distribution of field produces a noticeable broadening in individual lines of Zeeman pattern. Since, ferrites have cubic symmetry and the randomness of chemical disorder, the Eq. (5) will give rise to approximately equal probability for small quadrupole splitting of opposite sign, which results in net zero observable quadrupole splitting.

A large hyperfine field is present at B-site compared to A-site due to the presence of Fe^{3+} ions. The hyperfine interaction, results from the interactions of nucleus (or nuclei, in molecules) with internally generated electric and magnetic fields. The internal magnetic field of a nucleus can arise due to many interactions [32,33], and can be represented as:

$$H_{Int} = H_{Core} + H_{STHF} + H_{THF} + H_D \tag{6}$$

where the terms H_{Core}, H_{THF}, H_{STHF} and H_D represent the field due to polarization of s-electrons, transferred, super transferred fields and dipolar fields, respectively. It is seen that the value of internal magnetic fields decreases systematically at A and B-sites with an increase in Cu^{2+} ion concentration. The decrease in hyperfine field can be attributed to the effect of H_{STHF} and H_D whereas the value H_{Core} and H_{THF} do not vary with Cu^{2+} doping. The dipolar magnetic field decreases due to the replacement of Fe^{3+} ions of the higher magnetic moment ($5\mu_B$) by a paramagnetic Cu^{2+} ion having magnetic moment of $1\mu_B$ which effectively decreases the

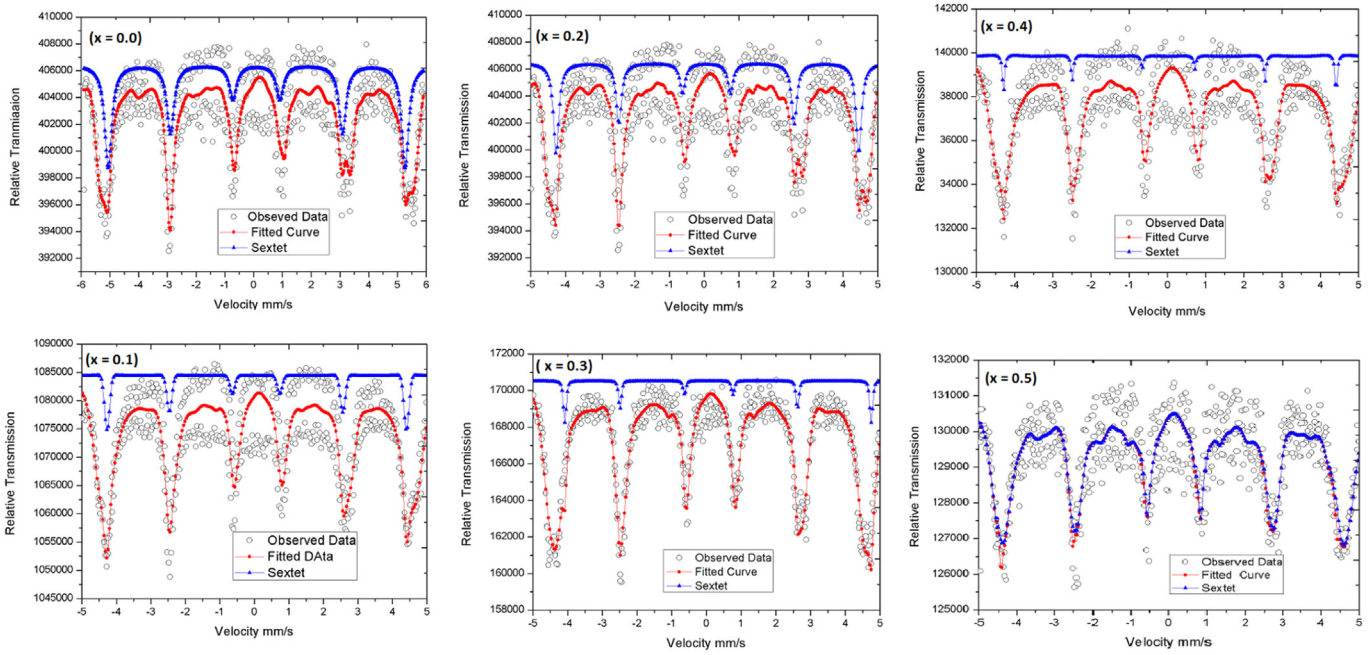

Fig. 6. Room temperature Mössbauer spectra of $CoFe_{2-x}Cu_xO_4$ ferrite nanoparticles for all compositions.

Table 2
Calculated Mössbauer parameters of $CoFe_{2-x}Cu_xO_4$ (x=0.0, 0.1, 0.2, 0.3, 0.4, and 0.5) ferrite nanoparticles.

(*x*)	Sub spectrum	WID 'Γ' (mm/s)	IS 'δ' (mm/s)	Hyperfine field 'H_f' (T)	Area (%)
0.0	(A)	0.281 (±0.01)	0.145(±0.003)	31.10 (±0.02)	99.90(±.001)
	(B)	0.0129(±0.46)	0.275(±0.002)	3.065(±0.04)	0.10(±0.01)
0.1	(A)	0.273(±0.002)	0.129(±0.002)	27.23(±0.024)	94.49(±0.01)
	(B)	0.194(±0.28)	0.060(±0.017)	26.96(±0.025)	5.51(±0.01)
0.2	(A)	0.188(±0.014)	0.144(±0.001)	27.81(±0.01)	80.93(±0.001)
	(B)	0.190(±0.11)	0.080(±0.008)	27.09(±0.01)	19.07(±0.001)
0.3	(A)	0.203(±0.009)	0.124(±0.003)	28.85(±0.022)	96.84(±0.001)
	(B)	0.076(±0.011)	0.200(±0.003)	27.43(±0.018)	3.16(±0.001)
0.4	(A)	0.610(±0.078)	0.125(±0.03)	29.16(±0.026)	97.55(±0.03)
	(B)	0.215(±0.010)	0.090(±0.004)	27.07(±0.037)	2.45(±0.05)
0.5	(A)	0.176(±0.19)	0.119(±0.006)	28.52(±0.059)	97.36(±0.003)
	(B)	0.092(±0.06)	0.0171(±0.007)	27.45(±0.024)	2.64(±0.06)

dipolar magnetic field H_D. Further, the reduction in the hyperfine fields can be related to particle size. The fluctuation of magnetization vectors in a direction close to an easy direction of magnetization leads to a particle size dependent magnetic hyperfine field. If the correlation time of the collective magnetization fluctuations is short relative to the observation time, the measured value of the magnetic field and consequently the hyperfine field will be reduced according to the equation:

$$H_{hf}(V, T) = H_{hf}(V = \infty, T)\left[1 - \frac{k_B T}{2KV}\right] \quad (7)$$

where k_B is the Boltzmann's constant, V is the particle volume and $V=\infty$, refers to a large crystal at temperature T in the absence of collective magnetic excitations. Therefore, according to above equation the hyperfine filed deceases with the decrease in particle size since particles with different volumes will show different hyperfine splitting.

4. Conclusions

Single phase nanoparticles of $CoFe_{2-x}Cu_xO_4$ mixed ferrites were prepared through auto combustion reaction method. The magnetic hysteresis curves show a reduction in saturation magnetization while the increase in coercivity up to 20%, followed by decreasing trend with increasing substitution of Cu^{2+} ions. The anisotropy constant, K_1, is found strongly dependent on composition of Cu^{2+} ions and has been explained on the basis of interparticle interaction and the distribution of cations over two sites. Mössbauer spectra shows two ferrimagnetically relaxed Zeeman sextets.

Acknowledgment

This project was funded by the National Plan for Science, Technology and Innovation (MAARIFAH), King Abdul Aziz City For Science and Technology, Kingdom of Saudi Arabia, Award Number (10NAN1999-02).

References

[1] C. Liu, A.J. Rondinone, Z.J. Zhang, J. Am. Chem. Soc. 122 (2000) 6263.
[2] J. Vejpravova, V. Sechovsky, J. Plocek, D. Niznansky, A. Hutlova, J.-

L. Rehsrpringer, J. Appl. Phys. 97 (2005) 124304.
[3] C. Kittel, Phys. Rev. 70 (1946) 965.
[4] R. Skmoshki, J. Phys.: Condens. Matter 15 (2003) R 841.
[5] S.A. Oliver, H.H. Hamdeh, J.C. Ho, Phys. Rev. B 60 (1999) 3400.
[6] H.H. Hamdeh, J.C. Ho, S.A. Oliver, R.J. Willey, G. Oliveri, G. Busca, J. Appl. Phys. 81 (1997) 1851.
[7] S. Dey, A. Roy, J. Ghosh, R.N. Bhowmik, R. Rangaathan, J. Appl. Phys. 90 (2001) 4138.
[8] L. Wang, F.S. Li, J. Magn. Magn. Mater. 223 (2001) 233.
[9] D. Yang, L.K. Lavoie, Y. Zhang, Z. Zhang, S. Ge, J. Appl. Phys. 93 (2003) 7492.
[10] T. Sugimoto, Synthesis, Characterization, and Mechanism of Growth, Marcel Dekker, New York, 2000.
[11] S. Chkoundali, S. Ammar, N. Jouini, F. Fievet, P. Molinie, M. Danot, F. Villain, J. M. Greneche, J. Appl. Phys. 90 (2001) 527.
[12] M. Rajenddran, R.C. Pulla, A.K. Bhattacharya, D. Das, S.N. Chintalapudi, C. K. Majumdar, J. Magn. Magn. Mater. 232 (2001) 71.
[13] S.E. Shirsath, M.L. Mane, Y. Yasukawa, X. Liu, A. Morisako, J. Nanopart. Res. 15 (2013) 1976.
[14] C. Liu, B. Zou, A.J. Rondinone, Z.J. Zhang, J. Am. Chem. Soc. 122 (2000) 6263.
[15] F. Hayama, S. Kitaoka, M. Kishimoto, H. Andoh, M. Amemiya, Ferrites, in: H. Wantanabe (Ed.), Proceedings of the Third International Conference Kyoto 1980, Center for Academic Publications, Japan, 1981, pp. 521.
[16] T.L. Tempeton, A.S. Arrott, A.E. Curzon, M.A. Gee, X.Z. Li, Y. Yoshida, P.J. Schurer, J.L. LaCombe, J. Appl. Phys. 73 (1993) 6728.
[17] N.S. Gajbhiye, S. Bhattacharyya, G. Balaji, R.S. Ningthoujam, R.K. Das, S. Basak, J. Weissmüller, Hyperfine Interact. 165 (2005) 153.
[18] A. Franco Jr., E.C.O. Lima, M.A. Noval, P. Well Jr., J. Magn. Magn. Mater. 308 (2007) 198.
[19] A. Franco Jr., V. Zapf, J. Magn. Magn. Mater. 320 (2008) 107.
[20] A.C.F.M. Costa, E. Tortella, M.R. Morelli, R.H.G.A. Kiminami, J. Magn. Magn. Mater. 256 (2003) 174.
[21] C.G. Koops, Phys. Rev. 83 (1951) 121–124.
[22] Sagar E. Shirsath, Santosh S. Jadhav, B.G. Toksha, S.M. Patange, K.M. Jadhav, Scr. Mater. 64 (2011) 773–776.
[23] G. Herzer, IEEE Trans. Magn. 26 (1990) 1397.
[24] L. Neel, Ann. Phys. 3 (1948) 137.
[25] Le Li, L. Peng, X. Zhu, D. Yang, J. Electr. Sci. Technol. 10 (2012) 88–92.
[26] N.S. Satya Murthy, M.G. Natera, Phys. Rev. 181 (1969).
[27] M.C. Dimri, A.K. Verma, S.C. Kashyap, D.C. Dube, O.P. Thakur, Mater. Sci. Eng. B 133 (1–3) (2006) 42–48.
[28] J. Smit, H.P.J. Wign, Ferrites, Wiley, New York, 1959.
[29] P.A. Jadhav, R.S. Devan, Y.D. Kolekar, B.K. Chougule, J. Phys. Chem. Solids 70 (2) (2009) 396–400.
[30] G. Kumar, J. Shah, R.K. Kotnala, V.P. Singh, Sarveena, G. Garg, Sagar E. Shirsath, K.M. Batoo, M. Singh, Mater. Res. Bull. 63 (2015) 216.
[31] E. Mathais, W. Schneider, R.M. Steffen, Phys. Rev. 125 (1962) 261.
[32] S. Verma, J. Chand, K.M. Batoo, M. Singh, J. Alloy. Compd. 51 (2013) 715.
[33] J. Chand, S. Verma, M. Singh, J. Alloy. Compd. 552 (2013) 715.